J. Water Environ. Nanotechnol., 10(3): 297-309 Summer 2025

ORIGINAL RESEARCH PAPER

Green Synthesis of Silver Nanoparticles Using green algae Pectin for Efficient Photocatalytic Activity

Mohammadali Pourmohammadi Mahunaki[1*], Mohammad Hadi Meshkatalsadat[2], Tayebeh Momeni[2]

[1] Department of Polymer Engineering, Faculty of Engineering, Qom University of Technology, Qom, Iran.
[2] Department of Chemistry, Qom University of Technology, Qom, Iran.

Received: 2024-12-19 Accepted: 2025-02-14 Published: 2025-08-01

ABSTRACT

This study utilized pectin extracted from green algae to synthesize environmentally friendly silver nanoparticles (AgNPs). The identity of the pectin was verified using Fourier transform infrared spectroscopy (FT-IR). A variety of methods, such as ultraviolet-visible spectroscopy (UV-Vis), field emission scanning electron microscopy (FE-SEM), transmission electron microscopy (TEM), X-ray diffraction (XRD), and FT-IR, were used to characterize the synthesized AgNPs. These characterizations revealed that the AgNPs were crystalline and had a spherical shape, with an average size of about 13 nm. The photocatalytic activity of the AgNPs was evaluated through the reduction of 4-nitrophenol (4-NP) and the degradation of methylene blue (MB). The reduction of 4-NP was observed using UV-Vis spectroscopy and was completed in just 15 minutes, while the degradation of MB was achieved within 10 minutes. These findings demonstrate the significant potential of pectin-based AgNPs for effectively removing organic pollutants. These pollutants are commonly found in industrial wastewater and pose significant environmental concerns.

Keywords: *Pectin, Algae, AgNPs, Photocatalysis, Methylene Blue, 4-Nitrophenol.*

How to cite this article
Pourmohammadi Mahunaki M.A., Meshkatalsadat M.H., Momeni T. Green Synthesis of Silver Nanoparticles Using green algae Pectin for Efficient Photocatalytic Activity. J. Water Environ. Nanotechnol., 2025; 10(3): 297-309.
DOI: 10.22090/jwent.2025.03.005

INTRODUCTION

A vast field of science and engineering known as "nanotechnology" manipulates and investigates materials at the nanoscale to study them. The field of nanotechnology involves the investigation and synthesis of materials with sizes between 1 and 100 nm. Due to their extremely small size, these nanoparticles (NPs), the foundation of nanotechnology, have unique features. These characteristics diverge significantly from bulk material properties [1; 2]. Among the diverse array of NPs, metal NPs have attracted noteworthy interest due to their remarkable magnetic, optical, mechanical, and electronic characteristics, paving the way for an extensive range of uses in numerous scientific and technological fields[3]. Because the materials employed in other conventional procedures are expensive and hazardous, attention has been drawn to the eco-friendly and economical way to synthesize nanoparticles. But the most economical, time- and money-efficient, environmentally friendly, and physiologically safe approach is green synthesis[4].

Silver nanoparticles (AgNPs) have attracted significant attention in this field due to their special properties, such as photocatalytic activity. Due to their exceptional electrical, optical, and antibacterial qualities, silver nanoparticles (AgNPs) are well-known in nanotechnology [5; 6]. AgNPs also have a large ratio of surface area-to-volume and

* Corresponding Author Email: *pourmohammadi@qut.ac.ir*

This work is licensed under the Creative Commons Attribution 4.0 International License.
To view a copy of this license, visit http://creativecommons.org/licenses/by/4.0/.

are frequently employed as catalysts in the photodegradation process[7]. On the other hand, traditional methods of producing AgNPs require harsh and hazardous chemicals, raising concerns about their detrimental environmental impacts. To pursue sustainable approaches, green synthesis methods for AgNPs have become a promising alternative. These methods use natural and environmentally friendly precursors to produce nanoparticles[2; 8]. Numerous phytocompounds found in plant extracts are used as capping and reducing agents during the synthesis of nanoparticles[9]. The primary phytocompounds that are accountable for the synthesis of AgNPs are flavonoids and antioxidant polyphenols. AgNPs are formed when silver ions are reduced from Ag+ to Ag. Additionally, flavonoids function as capping agents, stabilizing the size and shape of the formed nanoparticles during the synthesis process. Additionally, these phytocompounds tend to adsorb on nanoparticle surfaces[10; 11].

The plant extract concentration, temperature, PH, metal salt concentration, and reaction time all affect the rate, amount produced, and characteristics of the nanoparticles during the green synthesis of nanoparticles using plant extracts [12]. Various plant extracts, such as Lysiloma acapulcensis [13], Ocimum canum [14], Gymnema sylvestre leaf [15], Aerva lanata[16], Azadirachta indica [17], Benincasa hispida [18], Catharanthus roseus [19], Caesalpinia pulcherrima [20], Melissa officinalis [21], Pedalium murex [22], Parkia speciosa [23], Cotyledon orbiculata [24], Diospyros lotus [25], and Andean blackberry leaf [26], have been effectively reported regarding AgNPs biosynthesis. Green sea algae, remarkable organisms in the natural world, serve as a rich source of pectin. Pectin, a natural polysaccharide, serves as a stabilizing and reducing agent, offering a suitable replacement for harmful chemicals in AgNPs synthesis [27].

As industrialization progresses, there is increasing concern about the widespread discharge of dangerous materials into the environment. There are far more dyes, insecticides, phenols, and other organic pollutants with potentially hazardous consequences. Nitrophenols are among the most common contaminants found in wastewater [28]. Comparatively, methylene blue (MB), a cationic diazine dye, is extensively employed in various industrial applications. Practical methods are therefore currently required globally to remove these pollutants from industrial effluent [29]. Wastewaters containing organic pollutants have frequently been treated using chemical processes like oxidation and reduction, physical processes like adsorption, precipitation, reverse osmosis, and biological processes like aerobic and anaerobic intervention. One way to purify water is through photocatalytic degradation. Currently, biosynthesized nano-catalysts are commonly utilized to remove pollutants from water [30].

Despite previous studies on green synthesis of AgNPs, the use of pectin extracted from green sea algae for this purpose, particularly in the photocatalytic degradation of organic pollutants, remains a relatively under-investigated field, highlighting the need for further exploration. This study presents the following innovations:

- Utilizing pectin extracted from green sea algae for the synthesis of silver nanoparticles, which has been rarely investigated.
- Introducing a green, sustainable, and environmentally friendly method for AgNP production.
- Conducting a comprehensive structural, morphological, and physicochemical analysis of the synthesized nanoparticles.
- Evaluating the photocatalytic efficiency of the nanoparticles in degrading model organic pollutants such as 4-nitrophenol and methylene blue (MB) under light exposure.
- Developing an innovative approach with potential applications in water and wastewater treatment, clean energy production, and biomedical technologies.

EXPERIMENTAL SECTION

Materials

Green algae are collected from the Caspian Sea. The Merck Company provided the necessary materials for the extraction process, including 96% ethanol, sodium hydroxide, hydrochloric acid (37%), and silver nitrate ($AgNO_3$).

Several commonly used methods have also been employed to better understand and investigate nanoparticle properties, such as UV-Vis, XRD, FTIR, TEM, and SEM. UV-Vis

CC BY

spectral analysis was carried out using a Phystec-miniature UVS-2500 spectrophotometer. 1 nm resolution was obtained in the 190–800 nm range using a UV–visible absorption spectrophotometer. The Avatar Thermo Spectrophotometer system was used to record FT-IR spectra. The surface morphology and particle size were examined with a scanning electron microscope, the SEM FEI Quanta 200. Spectral analysis was utilized for the XRD (Philips PW 1730). The synthesized AgNPs' amorphous nature is confirmed through XRD analysis within the angle range of 20°–80° and X-ray diffraction analysis.

Preparing Pectin from sea algae

Step 1: Collection and Initial Preparation of Sea Algae

- Fresh sea algae were collected from the Caspian Sea in northern Iran.
- The algae were first washed with tap water to remove surface dirt and impurities.
- They were then washed again with deionized water to eliminate any remaining salts and particles.
- The cleaned algae were air-dried at ambient temperature.
- After drying, the algae were cut into small pieces to facilitate the extraction process.

Step 2: Preparation of the Extraction Mixture

- 50 grams of dried and chopped algae were placed in a 250 mL glass Erlenmeyer flask.
- 180 mL of deionized water was added to the dried algae.
- HCl (hydrochloric acid) was added to adjust the pH of the solution to 2.

Step 3: Pectin Extraction Using Ultrasonication

- The Erlenmeyer flask containing the mixture was placed in an ultrasonic device (Parsonic 2600; Iran).
- The sonication process was carried out for 22 minutes at a temperature of 70°C.
- During sonication, ultrasonic waves disrupted the cell walls of the algae, releasing the pectin.

Step 4: Pectin Precipitation

- After sonication, the Erlenmeyer flask was removed from the device and allowed to cool slightly.
- To precipitate the pectin, 96% ethanol was added to the extraction solution.
- The ratio of extraction solution to ethanol was 1:2.
- The mixture was left to rest at room temperature for 24 hours to allow complete precipitation of the pectin.

Filtration and Washing of Pectin

- After 24 hours, the solution was filtered through filter paper in a funnel to separate the precipitated pectin.
- The collected pectin was washed several times with 96% ethanol to remove impurities.

Step 6: Drying and Determining the Extraction Yield

- The precipitated pectin was dried in an oven at 60°C.
- After drying, the pectin was weighed to determine the amount extracted.
- From 50 grams of green sea algae, 12.53 grams of pure pectin were obtained.

Green synthesis of AgNPs

Commonly, an $AgNO_3$ aqueous solution and a pectin extract are utilized. The synthesis of nanoparticles happens at ambient temperature and completes in 30 minutes. In a glass Erlenmeyer flask, 90 mL of deionized water was combined with the required amount of $AgNO_3$ to prepare a 0.005 mM solution. The solution was stirred using a magnetic stirrer until the $AgNO_3$ was completely dissolved. Then, 10 g of pectin was added to the $AgNO_3$ solution (90 mL). The flask was left at room temperature for 30 minutes, during which the color changed from colorless to dark brown, showing that silver nanoparticles were forming. The nanoparticles were then separated and washed by centrifugation, and then allowed to dry in a 60°C oven.

Photo-catalytic degradation of MB dye by AgNPs

The photodegradation experiment involves preparing solutions of MB at a specific concentration and AgNP suspensions with varying concentrations (20, 40, 60, 80, and 100 mg/L). Reaction mixtures are then prepared by combining a fixed volume of the MB solution (10 mL) with varying volumes of the AgNP suspensions, and the final volumes are adjusted with deionized water to ensure consistency across all samples. These mixtures are kept for two hours in the dark to achieve adsorption equilibrium, and then exposed to a light source.

(cc) BY

At specific time intervals of 5, 10, 15, and 20 minutes, aliquots are taken from each reaction mixture, and their absorbance is measured. A UV-Vis spectrophotometer was used at the characteristic wavelength of MB to calculate the MB degradation efficiency.

Reduction of 4-nitrophenol

A quartz cell was filled with an aqueous solution of *4*-nitrophenol (0.005 M, 1 mL) and $NaBH_4$ (0.03 M, 1 mL). The reduction reaction was then started by adding 40 mg/L of the catalyst (convenient concentration). UV-Vis spectroscopy was used to monitor the reaction's progress every 0–10 minutes. At 318 nm, *4*-nitrophenol exhibits its most significant absorption peak. This peak shifts to 400 nm when $NaBH_4$ is added because a phenolate ion is formed. Following the phenolate ion reduction, the 400 nm peak flattens, and the 300 nm peak of the amine emerges. An absorption chart was plotted against the concentration chart to detect the response rate[31].

RESULTS AND DISCUSSION

FT-IR

The structure of pectin contains numerous -OH groups, as evidenced by the major peak in the 3200–3600 cm^{-1} range. The characteristic peaks of pectin were observed at 3377, 1538, 1343, 1234, and 991 cm^{-1}, each corresponding to specific functional groups. The 3377 cm^{-1} peak corresponds to the stretching vibrations of the O-H bond, indicative of hydroxyl groups in polysaccharides and absorbed water. The 1538 cm^{-1} peak is associated with the C=O stretching vibrations in carboxylate ($-COO^-$) groups, confirming the presence of ionized carboxyl groups in pectin. The 1343 cm^{-1} peak corresponds to the bending vibrations of the C-O-H bond, typical of carboxylic groups in polysaccharides, while the 1234 cm^{-1} peak represents C-O stretching vibrations in ester groups ($-COOCH_3$), indicating the presence of methoxy groups. Additionally, the 991 cm^{-1} peak is attributed to the C-O-C stretching vibrations, confirming the glycosidic linkages within the pectin polysaccharide structure. This analysis highlights the presence of hydroxyl (-OH), carboxylate ($-COO^-$), ester ($-COOCH_3$), and glycosidic (C-O-C) bonds, which define the complex polysaccharide nature of pectin [32; 33].

The FTIR spectrum in Fig. 1b corresponds to AgNPs synthesized using pectin, which acts as both a reducing and stabilizing agent. The observed shifts in peak positions and intensities compared to pure pectin confirm strong interactions between functional groups and silver nanoparticles. The broad peak at 3396.6 cm^{-1} corresponds to O-H stretching vibrations, indicating the presence of hydroxyl (-OH) groups in pectin, which play a crucial role in reducing Ag^+ to Ag^0 and stabilizing the nanoparticles. The peak at 1744.8 cm^{-1} is related to C=O stretching in ester (-COOR) groups, suggesting the interaction of pectin's methyl esters with AgNPs. The 1649.3 cm^{-1} peak, associated with C=O stretching in carboxylate ($-COO^-$) groups, signifies the involvement of carboxyl functional groups in the stabilization and capping of AgNPs. Additionally, 1387.9 cm^{-1} corresponds to C-H bending vibrations from the pectin polysaccharide backbone, while 1248.3 cm^{-1} represents C-O stretching in ester ($-COOCH_3$) and ether (C-O-C) groups, further confirming their role in stabilizing the nanoparticles. The 1086.6 cm^{-1} peak is attributed to C-O-C stretching vibrations, confirming the presence of glycosidic linkages in pectin, and the 829.4 cm^{-1} peak is linked to out-of-plane C-H bending vibrations in sugar rings, suggesting interactions between pectin and silver nanoparticles. These findings confirm that pectin effectively acts as both a reducing and stabilizing agent in AgNPs synthesis, with hydroxyl (-OH) and carboxylate ($-COO^-$) groups facilitating the reduction of Ag^+, while ester ($-COOCH_3$) and glycosidic (C-O-C) bonds aid in stabilization, ensuring the successful green synthesis of AgNPs. [34; 35].

UV–Vis

Figure 2 presents the UV-Vis spectra of silver nanoparticles (AgNPs) synthesized using pectin extracts. Upon adding the extract to the $AgNO_3$ solution, a visible color change from colorless to dark brown occurs. This color shift, indicative of AgNP synthesis, results from the collective oscillation of free conduction electrons caused by an electromagnetic field interacting with them, a phenomenon known as Surface Plasmon Resonance (SPR) excitation

CC BY

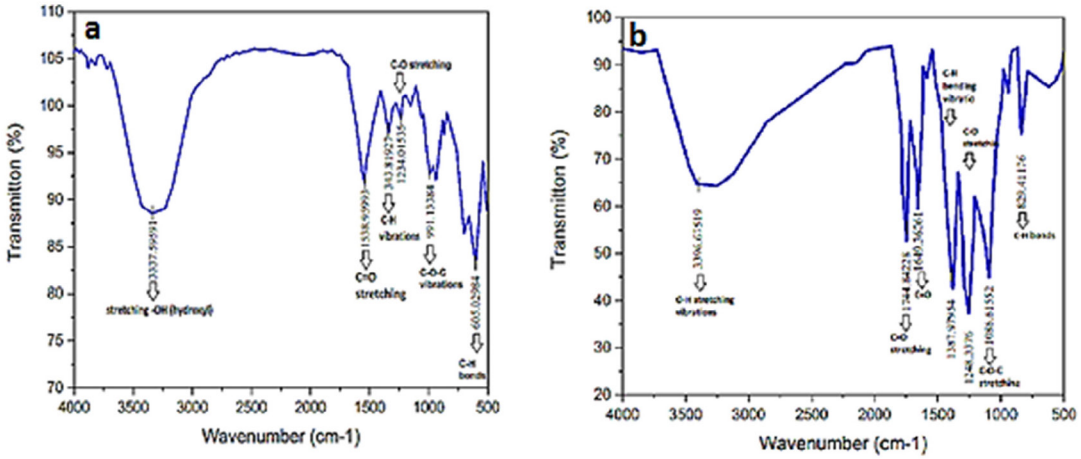

Fig. 1. Ft-IR spectrum of a) pectin and b) AgNPs.

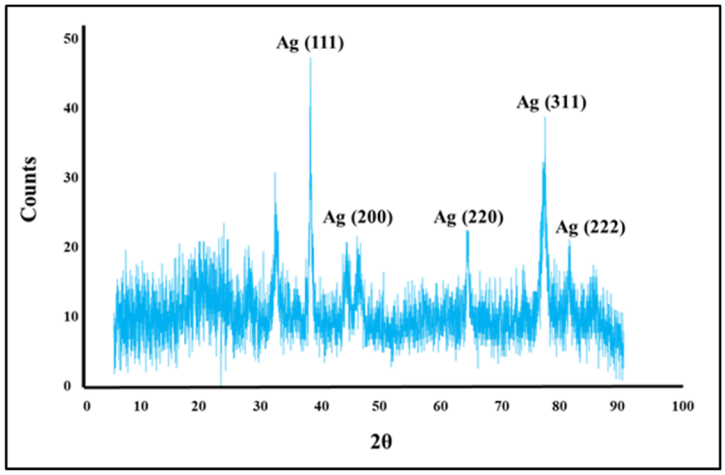

Fig. 3. XRD pattern of AgNPs.

[36]. All extracts successfully produced AgNPs, as evidenced by the distinct absorbance peaks observed between 432 and 450 nm in Figure 2. The SPR peak at approximately 432–450 nm corresponds to the collective oscillation of conduction electrons in AgNPs when excited by light, serving as a key indicator of nanoparticle formation and confirming their presence in the colloidal solution. The position and intensity of the SPR peak are influenced by factors such as particle size, shape, and aggregation state. A peak within this range typically indicates the presence of small, spherical AgNPs, while broader or red-shifted peaks suggest particle aggregation or larger nanoparticles.

The natural biomolecules in pectin, including hydroxyl (-OH) and carboxyl ($-COO^-$) groups, facilitate the reduction of Ag^+ to AgNPs and stabilize them, preventing excessive aggregation. The smooth and symmetric SPR peak suggests that the nanoparticles are well-dispersed with minimal aggregation. Furthermore, the absence of peaks beyond 500 nm confirms that the nanoparticles remain monodisperse and stable, highlighting the efficient capping and stabilization role of pectin in AgNP synthesis [37-39]. This absorption range (400-450 nm) is consistent with previously reported SPR peaks for AgNPs. The presence of these peaks confirms the successful formation of AgNPs [40].

XRD

The green synthesis of AgNPs' crystal structure was ascertained using the XRD

CC BY

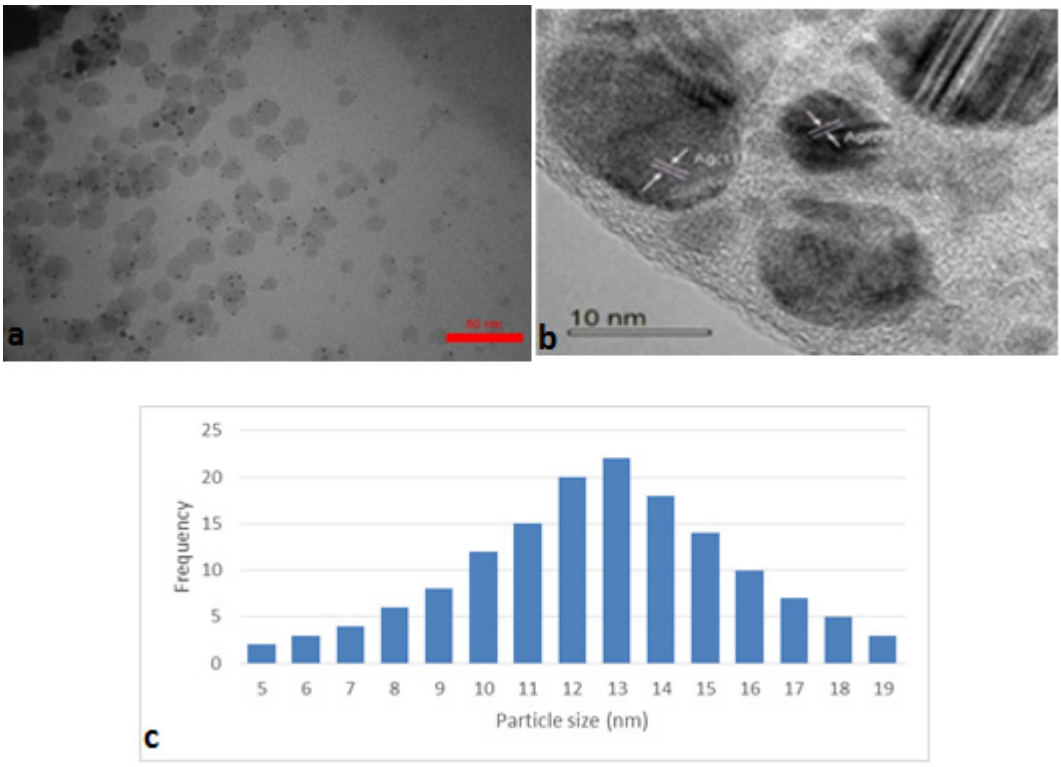

Fig. 4. TEM analysis of AgNPs (a) 50 nm (b) 10nm and (c) average size of 13nm.

method. The pattern of XRD for the current green synthetic AgNPs is shown in Fig. 3. Some Bragg reflections are found, which can be used to index the bands for AgNPs' face-centered cubic (fcc) structures. These reflections have 2Θ values of 38.65, 45.31, 61.35, and 77.12, respectively, corresponding to the sets of lattice planes (111), (200), (220), and (311). The (111) plane has more intensity than the other planes. JCPDS data card no. 96-900-8460 provided confirmation of the values of the diffraction peak and lattice constant. When the diffraction peaks are at half-maximum, to find the average crystallite size throughout the breadth, the Debye-Scherrer equation is applied [41].

$$D = \frac{0.9\lambda}{\beta cos\theta}$$

β (in radians) represents the full width at half maximum (FWHM) of the diffraction peak in the Debye-Scherrer equation. The X-ray wavelength (1.54056 Å) is represented by λ, whereas D represents grain size. Using XRD measurements, the size of the crystallites was 12 ± 2.3 nm. AgNPs synthesized using the green method undoubtedly exhibit a nanocrystalline nature, as evidenced by unique structural peaks in the XRD patterns. These XRD patterns are consistent with previous studies of AgNPs produced using environmentally friendly processes [42-44].

TEM

Silver nanoparticles (AgNPs) were characterized using transmission electron microscopy (TEM). TEM is one of the most advanced imaging tools for determining the size, shape, and morphology of nanoparticles [45]. TEM images of the synthesized products confirm the presence of silver nanoparticles as dispersed dark spots against a lighter background. These images, captured within a range of 10 and 50 nm, indicate that the average size of the nanoparticles is 13 nm, with a noticeable size distribution.

While confirming their colloidal nature solely through TEM images is challenging, the appropriate dispersion and lack of severe aggregation suggest potential stabilization, likely due to residual organic matter such as

CC BY

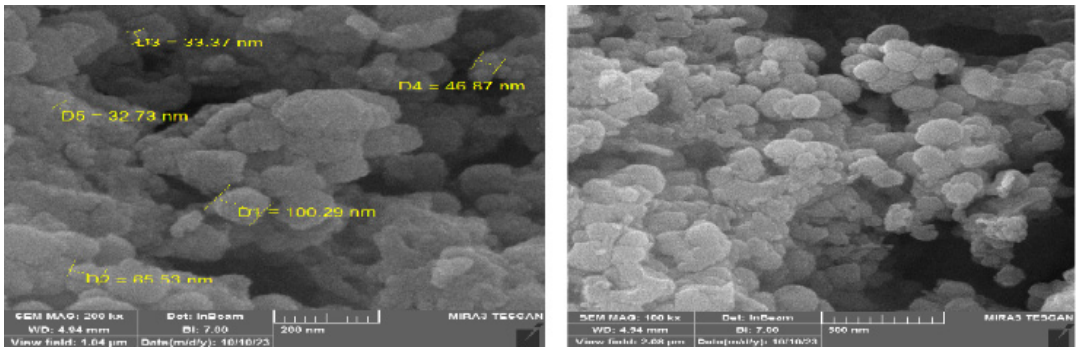

Fig. 5. FE-SEM image of AgNPs.

pectin. The slightly hazy regions around some nanoparticles indicate the presence of these residual organic materials, which may influence their stability and properties. Additionally, the images reveal a wide dispersion and some degree of irregularity in the shape of the spherical nanoparticles.

To better examine the size distribution, a histogram was plotted, showing that most nanoparticles fall within the 13 nm range. This relatively broad distribution suggests variations in particle size, which align with TEM observations. These findings indicate that the nanoparticle system is well-dispersed and likely stabilized by organic matter.

FE-SEM

Using FE-SEM analysis, morphology, surface homogeneity, and particle size may all be examined. Fig. 5 shows microscopy pictures of manufactured AgNPs at various concentrations of silver precursor. According to FE-SEM analyses, the nanoparticles' typical diameters range from 32 to 100 nm, and their surface shape is spherical. FE-SEM images show that the nanoparticles are homogeneous and do not show significant aggregation.

PHOTOCATALYTIC ACTIVITY

Methylene blue dye photocatalytic degradation by AgNPs

The ability of metal nanoparticles to catalyze processes that would not otherwise be possible is one of their primary uses. The catalytic activity of nanoparticles is strongly influenced by their composition, size, and shape. Higher catalytic activity is generally indicated by a larger surface-to-volume ratio [46]. It is commonly known that during the dye reduction and removal process, AgNPs exhibit enhanced catalytic activity. The textile industry has recently seen a rise in the use of MB, a heterocyclic aromatic dye. The process above produced AgNPs, which were then utilized as a catalyst by $NaBH_4$ to reduce MB.

A spectrophotometer was used to evaluate the AgNPs' photocatalytic efficacy on the MB dye. In its oxidized condition, MB is blue; however, when reduced to MB, it becomes colorless. To investigate the photocatalytic effect of AgNPs on MB degradation, solutions containing a constant concentration of MB and varying concentrations of AgNPs (20, 40, 60, 80, and 100 mg/L) were used. After 25 minutes, the intensity of the absorption spectra for every solution was determined using UV-Vis spectroscopy. Figure 6a displays the UV-Vis absorption spectra of MB reduction without a catalyst (AgNPs). The UV-Vis absorption spectra of MB reduction with increasing concentrations of the synthesized catalyst are displayed in Fig. 6b. It was found from the data that as the AgNP concentration rises, MB absorption strength falls. Because a higher concentration of AgNPs provides more accessible and active sites on the catalyst's surface, leading to an increase in hydroxyl radicals involved in the process. The absorption maxima of MB in an aqueous solution are often observed at 663 nm due to the π/π^* and n/π^* transitions[47]. The highest absorption band at 663 nm will diminish as the catalytic degradation proceeds; in comparison, a new band with a maximum of 432 nm will simultaneously develop and become more intense with time. Notably, the reduction of MB was completed in just 10 minutes in the

CC BY

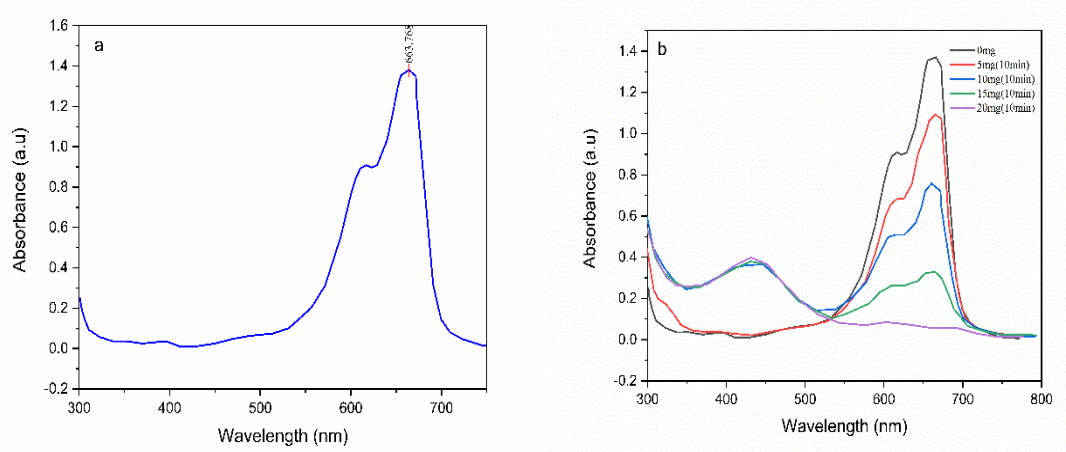

Fig. 6. UV-Vis spectrum of a) without AgNPs b) with different concentration solutions of AgNPs Under the photocatalytic system.

Table 1. Comparing the MB reduction time in the presence of AgNPs synthesized from plant extract.

NO	Catalyst	Time	Reference
1	AgNPs/ Polygonum Hydropiper	13 min	**[50]**
2	AgNPs/Gmelina arborea	10 min	**[51]**
3	AgNPs / Marine Algae	20 min	**[52]**
4	AgNPs/ Alchemilla vulgaris Helichrysum arenarium	6-7 min	**[29]**
5	This work	10 min	-

presence of 20 mg/L of AgNPs.

A comparison of our findings with previous data on the duration required to attain 100% MB color reduction using AgNPs derived from a plant extract is shown in Table 1. AgNPs assist in the catalytic breakdown of MB, with a potential mechanism described by the Langmuir-Hinshelwood model[48]. Here, $NaBH_4$ acts as a supply of hydrogen and an electron donor. It serves as an intermediary to transport electrons between the BH^-_4 ion and the MB due to its high damaging potential (-1.8 V vs. NHE) [49]. Instantaneous electron and hydrogen transfer occurs when $NaBH_4$ is added to a solution containing AgNPs and MB. This occurs due to the BH_4^- ion from the MB and $NaBH_4$ molecules adhering to the AgNPs' surface. The colorless degraded by-product that results from diffusion between adsorbed molecules desorbs. AgNPs' wide surface area may provide more catalytic sites for the breakdown of MB. These results show that adding AgNPs in the right amount increases the efficiency of the MB reduction reaction. These findings imply that the colloidal AgNPs produced serve as an efficient "green catalyst," mediating electron transport during the reduction of MB. As a green catalyst, AgNPs act as electron transfer mediators, facilitating the movement of electrons from BH_4^- to MB, leading to its reduction into a colorless product. The high surface area of AgNPs enhances contact between reactant molecules, increasing catalytic efficiency. This process occurs without toxic chemical additives, making AgNPs an eco-friendly alternative to traditional chemical catalysts. Additionally, optimizing the amount of AgNPs is crucial, as an inadequate concentration may lead to a slow reaction, while an excessive amount might cause nanoparticle aggregation, reducing the available catalytic sites. Therefore, the efficient electron transfer, high catalytic activity, and eco-friendly nature of AgNPs confirm their role as a promising green catalyst for the degradation of organic pollutants like MB.

Catalytic activities of AgNPs in the 4-nitrophenol

Industries release combinations of phenol and nitroaromatic chemicals that are highly harmful to human health [53; 54]. Nitrophenolic compounds and their derivatives

CC BY

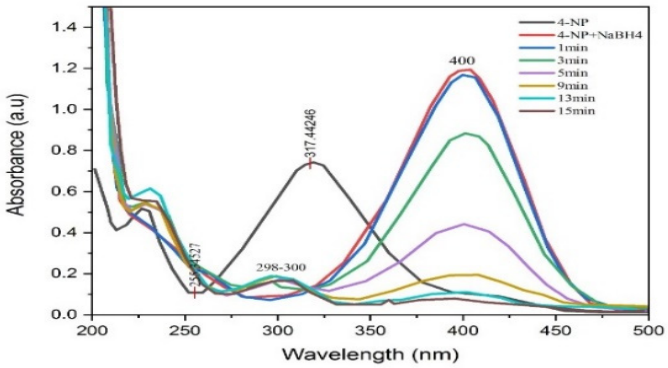

Fig. 7 Reduced 4-NP catalytically by AgNPs.

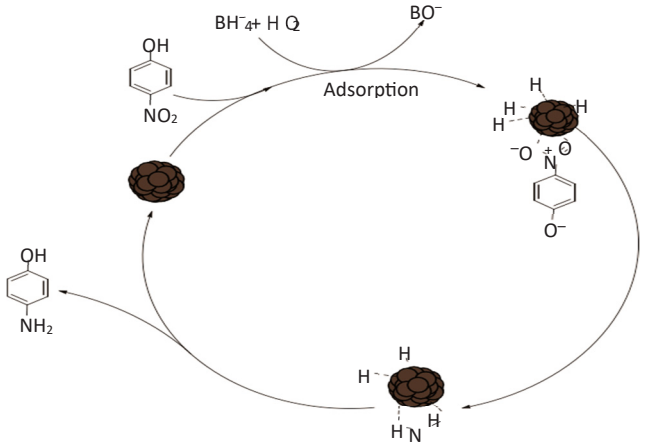

Scheme 1 Mechanism of Catalytic reduction reaction of 4-NP into 4-AM using AgNPs.

are specifically produced during the production of herbicides, insect repellents, and insecticides [55]. The *4*-NP must be transformed into valuable compounds like *4*-aminophenol (*4*-AP) to reduce its toxicity. In this work, *4*-NP was catalytically reduced to *4*-AP using green synthetic AgNPs. Green synthesis AgNPs were utilized as a catalyst to remove the kinetic barrier that slowed the transfer of electrons from the donor (BH4-) to the acceptor, 4-NP. As shown in Fig. 7, a strong peak that *4*-NP displayed at 317 nm was shifted to 400 nm using $NaBH_4$, and the absorbance at 400 nm was used to measure the reduction process. At 400 nm, a steady decline in absorbance was seen, and after adding the reaction mix containing the biosynthesized AgNPs. Similarly, during 5 minutes at 298 nm, the peak intensity increased. The complete reduction of *4*-NP dye, evidenced by the disappearance of its yellow color, was achieved within 15 minutes under UV light irradiation. This suggests the successful 4-NP to 4-AP conversion. The proposed reaction mechanism for this photocatalytic reduction involves four key steps: (I) Hydrogen from the BH_4^- ion is adsorbed onto the surface of the AgNPs. (II) The surface of the AgNPs absorbs the 4-NP dye molecules. (III) As a bridge, AgNPs help electrons move from the donor, the BH_4^- ion, to the acceptor, the *4*-NP molecule. (ÉV) The reduced *4*-AP desorbs from the AgNPs surface (Scheme 1)[56]. The reaction time for 4-NP degradation has been compared with previous studies (Table 2).

The Reusability and Catalytic Efficiency of AgNPs in the Degradation of MB and 4-NP

To assess the reusability of AgNPs in the degradation of MB and 4-NP, multiple reaction cycles should be conducted to evaluate the

CC BY

Table 2. Comparing the 4-NP reduction time in the presence of AgNPs made from plant extract.

NO	Catalyst	Time	Reference
1	AgNPs/Sun-dried tulsi leaves	30 min	**[57]**
2	AgNPs/ Allium ampeloprasum L. leaf	12 min	**[58]**
3	This work	15 min	-

Table 3. Reusability Evaluation of AgNPs in the Degradation of MB and 4-NP.

Cycle	AgNPs Concentration (mg/L)	Color Reduction Rate (after each cycle)	Time Required for Complete MB Reduction	Time Required for Complete 4-NP Reduction	Change in Reaction Rate	Result
1	20	90%	10 minutes	15 minutes	-	Active Catalyst
2	20	80%	12 minutes	18 minutes	Slight decrease	Fairly Active Catalyst
3	20	65%	15 minutes	23minutes	Significant decrease	Catalytic Activity Reduced
4	20	40%	18 minutes	28 minutes	Further decrease	Loss of Catalytic Activity
5	20	20%	20 minutes	40minutes	Severe decrease	Loss of Catalytic Activity

catalytic performance of these nanoparticles in both processes. After each cycle, the AgNPs can be separated from the solution and reused in a new reaction mixture. The catalytic efficiency is determined by measuring the rate of color reduction and the color changes in the solutions. A decline in catalytic efficiency, accompanied by a slower reaction rate over successive cycles, suggests a reduction in the catalyst's effectiveness.

The results from the table show that AgNPs reduce MB and 4-NP at high speed and excellent efficiency in the first cycle. However, as the number of cycles increases, both the rate of color reduction and the time required for complete reduction of both pollutants increase. In cycles 2 and 3, a slight decrease in catalytic efficiency is observed, indicating a gradual reduction in the effectiveness of AgNPs. In cycles 4 and 5, a significant decrease in catalytic efficiency leads to the loss of catalytic activity. This reduction in performance could be due to nanoparticle aggregation, structural degradation, or leaching of silver ions into the solution, which negatively impacts the efficiency and stability of the catalyst.

CONCLUSIONS

This study explored the potential of pectin extracted from algae for the green synthesis of AgNPs. The FT-IR analysis confirmed successful pectin extraction. The generated AgNPs had a crystalline structure and spherical morphology, as determined by UV-Vis, FT-IR, FE-SEM, XRD, and TEM analyses. This eco-friendly synthesis approach offers advantages like scalability and cost-effectiveness. The synthesized Ag-NPs demonstrated remarkable efficiency as a photocatalyst in degrading MB and as a catalyst in reducing *4*-NP. Key advantages of these AgNPs include easy separation, high catalytic efficiency, excellent stability, and reusability without significant activity loss. These results indicate that these nanoparticles can be applied in water and wastewater treatment to eliminate recalcitrant organic pollutants.

The scalability limitations require further investigation for industrial-scale applications, and the impact of these nanoparticles under different environmental conditions and temperatures should also be evaluated. Additionally, the efficiency of silver nanoparticles in the presence of other pollutants and their ability to remove combined pollutants should be studied. Furthermore, assessing their long-term stability and environmental impacts in industrial and environmental applications is crucial. These issues can provide the basis for future research on the use of silver nanoparticles as a green catalyst in water and wastewater treatment

(cc) BY

and other industrial applications.

CONFLICT OF INTEREST

The authors declare no conflict of interest.

REFERENCES

1. Fouad DE, Zhang C, El-Didamony H, Yingnan L, Mekuria TD, Shah AH. Improved size, morphology and crystallinity of hematite (α-Fe_2O_3) nanoparticles synthesized via the precipitation route using ferric sulfate precursor. Results Phys. 2019;12:1253-61. https://doi.org/10.1016/j.rinp.2019.01.005
2. Kalpana D, Han JH, Park WS, Lee SM, Wahab R, Lee YS. Green biosynthesis of silver nanoparticles using Torreya nucifera and their antibacterial activity. Arab J Chem. 2019;12:1722-32. https://doi.org/10.1016/j.arabjc.2014.08.016
3. Begum NA, Mondal S, Basu S, Laskar RA, Mandal D. Biogenic synthesis of Au and Ag nanoparticles using aqueous solutions of Black Tea leaf extracts. Colloids Surf B Biointerfaces. 2009;71:113-8. https://doi.org/10.1016/j.colsurfb.2009.01.012
4. Asghar MA, Asghar MA. Green synthesized and characterized copper nanoparticles using various new plants extracts aggravate microbial cell membrane damage after interaction with lipopolysaccharide. Int J Biol Macromol. 2020;160:1168-76. https://doi.org/10.1016/j.ijbiomac.2020.05.198
5. Ameen F, Abdullah MM, Al-Homaidan AA, Al-Lohedan HA, Al-Ghanayem AA, Almansob A. Fabrication of silver nanoparticles employing the cyanobacterium Spirulina platensis and its bactericidal effect against opportunistic nosocomial pathogens of the respiratory tract. J Mol Struct. 2020;1217:128392. https://doi.org/10.1016/j.molstruc.2020.128392
6. Wasilewska A, Klekotka U, Zambrzycka M, Zambrowski G, Święcicka I, Kalska-Szostko B. Physico-chemical properties and antimicrobial activity of silver nanoparticles fabricated by green synthesis. Food Chem. 2023;400:133960. https://doi.org/10.1016/j.foodchem.2022.133960
7. Yu SJ, Yin YG, Liu JF. Silver nanoparticles in the environment. Environ Sci Process Impacts. 2013;15:78-92. https://doi.org/10.1039/C2EM30595J
8. Fouad DE, Zhang C, Mekuria TD, Bi C, Zaidi AA, Shah AH. Effects of sono-assisted modified precipitation on the crystallinity, size, morphology, and catalytic applications of hematite (α-Fe_2O_3) nanoparticles: A comparative study. Ultrason Sonochem. 2019;59:104713. https://doi.org/10.1016/j.ultsonch.2019.104713
9. Chand K, Cao D, Fouad DE, Shah AH, Dayo AQ, et al. Green synthesis, characterization and photocatalytic application of silver nanoparticles synthesized by various plant extracts. Arab J Chem. 2020;13:8248-61. https://doi.org/10.1016/j.arabjc.2020.01.009
10. Shaik MR, Khan M, Kuniyil M, Al-Warthan A, Alkhathlan HZ, et al. Plant-extract-assisted green synthesis of silver nanoparticles using Origanum vulgare L. extract and their microbicidal activities. Sustainability. 2018;10:913. https://doi.org/10.3390/su10040913
11. Swilam N, Nematallah KA. Polyphenols profile of pomegranate leaves and their role in green synthesis of silver nanoparticles. Sci Rep. 2020;10:14851. https://doi.org/10.1038/s41598-020-71847-5
12. Behravan M, Panahi AH, Naghizadeh A, Ziaee M, Mahdavi R, Mirzapour A. Facile green synthesis of silver nanoparticles using Berberis vulgaris leaf and root aqueous extract and its antibacterial activity. Int J Biol Macromol. 2019;124:148-54. https://doi.org/10.1016/j.ijbiomac.2018.11.101
13. Garibo D, Borbón-Nuñez HA, de León JND, García Mendoza E, Estrada I, et al. Green synthesis of silver nanoparticles using Lysiloma acapulcensis exhibit high-antimicrobial activity. Sci Rep. 2020;10:12805. https://doi.org/10.1038/s41598-020-69606-7
14. Tailor G, Yadav B, Chaudhary J, Joshi M, Suvalka C. Green synthesis of silver nanoparticles using Ocimum canum and their anti-bacterial activity. Biochem Biophys Rep. 2020;24:100848. https://doi.org/10.1016/j.bbrep.2020.100848
15. Rajkumar P, Prakasam A, Rajeshkumar S, Gomathi M, Anbarasan P, Chandrasekaran R. Green synthesis of silver nanoparticles using Gymnema sylvestre leaf extract and evaluation of its antibacterial activity. S Afr J Chem Eng. 2020;32:1-4. https://doi.org/10.1016/j.sajce.2019.11.005
16. Kanniah P, Radhamani J, Chelliah P, Muthusamy N, Joshua Jebasingh Sathiya Balasingh Thangapandi E, et al. Green synthesis of multifaceted silver nanoparticles using the flower extract of Aerva lanata and evaluation of its biological and environmental applications. ChemistrySelect. 2020;5:2322-31. https://doi.org/10.1002/slct.201903228
17. Alharbi NS, Alsubhi NS. Green synthesis and anticancer activity of silver nanoparticles prepared using fruit extract of Azadirachta indica. J Radiat Res Appl Sci. 2022;15:335-45. https://doi.org/10.1016/j.jrras.2022.08.009
18. Soliman WE, Khan S, Rizvi SMD, Moin A, Elsewedy HS, et al. Therapeutic applications of biostable silver nanoparticles synthesized using peel extract of Benincasa hispida: Antibacterial and anticancer activities. Nanomaterials (Basel). 2020;10:1954. https://doi.org/10.3390/nano10101954
19. Kandiah M, Chandrasekaran KN. Green synthesis of silver nanoparticles using Catharanthus roseus flower extracts and the determination of their antioxidant, antimicrobial, and photocatalytic activity. J Nanotechnol. 2021;2021:5512786. https://doi.org/10.1155/2021/5512786
20. Moteriya P, Chanda S. Green synthesis of silver nanoparticles from Caesalpinia pulcherrima leaf extract and evaluation of their antimicrobial, cytotoxic and genotoxic potential (3-in-1 system). J Inorg Organomet Polym Mater. 2020;30:3920-32. https://doi.org/10.1007/s10904-020-01532-7
21. Motafeghi F, Gerami M, Mortazavi P, Khayambashi B, Ghassemi-Barghi N, Shokrzadeh M. Green synthesis of silver nanoparticles, graphene, and silver-graphene nanocomposite using Melissa officinalis ethanolic extract: Anticancer effect on MCF-7 cell line. Iran J Basic Med Sci. 2023;26:57.
22. Balan L, Chandrasekaran S, Gajendiran M, Nanjian R. Synthesis of silver nanoparticles from Pedalium murex L. and its antiproliferative activity against breast cancer (MCF-7) cells. J Mol Struct. 2021;1242:130695. https://doi.org/10.1016/j.molstruc.2021.130695
23. Kikon L, Sumedha N, Rajaganesh K, Chamuah J, Rupreo V, et al. Green synthesis of silver nanoparticles from Parkia speciosa seeds and pods extract: Characterization and antioxidant properties for biomedical and nanotechnological applications. Biochem Cell Arch. 2024;24. https://doi.org/10.51470/bca.2024.24.1.405
24. Tyavambiza C, Elbagory AM, Madiehe AM, Meyer M, Mey-

CC BY

er S. The antimicrobial and anti-inflammatory effects of silver nanoparticles synthesised from Cotyledon orbiculata aqueous extract. Nanomaterials (Basel). 2021;11:1343. https://doi.org/10.3390/nano11051343
25. Yasmin S, Nouren S, Bhatti HN, Iqbal DN, Iftikhar S, et al. Green synthesis, characterization and photocatalytic applications of silver nanoparticles using Diospyros lotus. Green Process Synth. 2020;9:87-96. https://doi.org/10.1515/gps-2020-0010
26. Herrera EM, Lucio S, Izquierdo A, Arroyo G, Stael C, Toulkeridis T. Application of multicomponent nanoparticles synthesized with Andean blackberry fruit extract (Rubus glaucus) NPs (Ca, Fe, Mg-Rg) for oyster mushrooms (Pleurotus ostreatus). In: Proc XVIII Multidiscip Int Congr Sci Technol. Springer; 2023. p.149-62. https://doi.org/10.1007/978-3-031-52258-1_11
27. Su DL, Li PJ, Ning M, Li GY, Shan Y. Microwave assisted green synthesis of pectin based silver nanoparticles and their antibacterial and antifungal activities. Mater Lett. 2019;244:35-8. https://doi.org/10.1016/j.matlet.2019.02.059
28. Das TK, Ghosh SK, Das NC. Green synthesis of a reduced graphene oxide/silver nanoparticles-based catalyst for degradation of a wide range of organic pollutants. Nano Struct Nano Objects. 2023;34:100960. https://doi.org/10.1016/j.nanoso.2023.100960
29. Kahraman HT. Synthesis of silver nanoparticles using Alchemilla vulgaris and Helichrysum arenarium for methylene blue and 4-nitrophenol degradation and antibacterial applications. Biomass Convers Biorefinery. 2024:1-12. https://doi.org/10.1007/s13399-024-05314-w
30. Das TK, Remanan S, Ghosh S, Ghosh SK, Das NC. Efficient synthesis of catalytic active silver nanoparticles illuminated cerium oxide nanotube: A mussel inspired approach. Environ Nanotechnol Monit Manag. 2021;15:100411. https://doi.org/10.1016/j.enmm.2020.100411
31. Das TK, Bhawal P, Ganguly S, Mondal S, Das NC. A facile green synthesis of amino acid boosted Ag decorated reduced graphene oxide nanocomposites and its catalytic activity towards 4-nitrophenol reduction. Surf Interfaces. 2018;13:79-91. https://doi.org/10.1016/j.surfin.2018.08.004
32. Monsoor M, Kalapathy U, Proctor A. Determination of polygalacturonic acid content in pectin extracts by diffuse reflectance Fourier transform infrared spectroscopy. Food Chem. 2001;74:233-8. https://doi.org/10.1016/S0308-8146(01)00100-5
33. Kar F, Arslan N. Characterization of orange peel pectin and effect of sugars, L-ascorbic acid, ammonium persulfate, salts on viscosity of orange peel pectin solutions. Carbohydr Polym. 1999;40:285-91. https://doi.org/10.1016/S0144-8617(99)00063-6
34. Paosen S, Saising J, Septama AW, Voravuthikunchai SP. Green synthesis of silver nanoparticles using plants from Myrtaceae family and characterization of their antibacterial activity. Mater Lett. 2017;209:201-6. https://doi.org/10.1016/j.matlet.2017.07.102
35. Kumar B, Smita K, Cumbal L, Debut A. Green synthesis of silver nanoparticles using Andean blackberry fruit extract. Saudi J Biol Sci. 2017;24:45-50. https://doi.org/10.1016/j.sjbs.2015.09.006
36. Raghunandan D, Bedre MD, Basavaraja S, Sawle B, Manjunath S, Venkataraman A. Rapid biosynthesis of irregular shaped gold nanoparticles from macerated aqueous extracellular dried clove buds (Syzygium aromaticum) solution. Colloids Surf B Biointerfaces. 2010;79:235-40. https://doi.org/10.1016/j.colsurfb.2010.04.003
37. GnanaJobitha G, Annadurai G, Kannan C. Green synthesis of silver nanoparticle using Elettaria cardamomom and assessment of its antimicrobial activity. Int J Pharm Sci Res. 2012;3:323-30.
38. Bogireddy NKR, Kumar HAK, Mandal BK. Biofabricated silver nanoparticles as green catalyst in the degradation of different textile dyes. J Environ Chem Eng. 2016;4:56-64. https://doi.org/10.1016/j.jece.2015.11.004
39. de Aragao AP, de Oliveira TM, Quelemes PV, Perfeito MLG, Araujo MC, et al. Green synthesis of silver nanoparticles using the seaweed Gracilaria birdiae and their antibacterial activity. Arab J Chem. 2019;12:4182-8. https://doi.org/10.1016/j.arabjc.2016.04.014
40. Gopinath V, Priyadarshini S, Loke MF, Arunkumar J, Marsili E, et al. Biogenic synthesis, characterization of antibacterial silver nanoparticles and its cell cytotoxicity. Arab J Chem. 2017;10:1107-17. https://doi.org/10.1016/j.arabjc.2015.11.011
41. Borchert H, Shevchenko EV, Robert A, Mekis I, Kornowski A, et al. Determination of nanocrystal sizes: a comparison of TEM, SAXS, and XRD studies of highly monodisperse $CoPt_3$ particles. Langmuir. 2005;21:1931-6. https://doi.org/10.1021/la0477183
42. Philip D. Green synthesis of gold and silver nanoparticles using Hibiscus rosa sinensis. Phys E Low Dimens Syst Nanostruct. 2010;42:1417-24. https://doi.org/10.1016/j.physe.2009.11.081
43. Bar H, Bhui DK, Sahoo GP, Sarkar P, Pyne S, Misra A. Green synthesis of silver nanoparticles using seed extract of Jatropha curcas. Colloids Surf A Physicochem Eng Asp. 2009;348:212-6. https://doi.org/10.1016/j.colsurfa.2009.07.021
44. Shankar SS, Ahmad A, Sastry M. Geranium leaf assisted biosynthesis of silver nanoparticles. Biotechnol Prog. 2003;19:1627-31. https://doi.org/10.1021/bp034070w
45. Ravichandran V, Vasanthi S, Shalini S, Shah SAA, Tripathy M, Paliwal N. Green synthesis, characterization, antibacterial, antioxidant and photocatalytic activity of Parkia speciosa leaves extract mediated silver nanoparticles. Results Phys. 2019;15:102565. https://doi.org/10.1016/j.rinp.2019.102565
46. Daniel MC, Astruc D. Gold nanoparticles: assembly, supramolecular chemistry, quantum-size-related properties, and applications toward biology, catalysis, and nanotechnology. Chem Rev. 2004;104:293-346. https://doi.org/10.1021/cr030698+
47. Faezeh F, Sara H. Facile synthesis and characterization of nanoporous NiO with folic acid as photodegradation catalyst for Congo red. Mater Sci Appl. 2012;2012.
48. Panáček A, Prucek R, Hrbáč J, Nevečná TJ, Šteffková J, et al. Polyacrylate-assisted size control of silver nanoparticles and their catalytic activity. Chem Mater. 2014;26:1332-9. https://doi.org/10.1021/cm400635z
49. Edison TNJI, Lee YR, Sethuraman MG. Green synthesis of silver nanoparticles using Terminalia cuneata and its catalytic action in reduction of direct yellow-12 dye. Spectrochim Acta A Mol Biomol Spectrosc. 2016;161:122-9. https://doi.org/10.1016/j.saa.2016.02.044
50. Bonnia N, Kamaruddin M, Nawawi M, Ratim S, Azlina H, Ali E. Green biosynthesis of silver nanoparticles using Polygonum hydropiper and study its catalytic degradation of methylene blue. Procedia Chem. 2016;19:594-602. https://

doi.org/10.1016/j.proche.2016.03.058
51. Shi H, Yu Y, Zhang Y, Feng X, Zhao X, et al. Polyoxometalate/TiO_2/Ag composite nanofibers with enhanced photocatalytic performance under visible light. Appl Catal B Environ. 2018;221:280-9. https://doi.org/10.1016/j.apcatb.2017.09.027
52. Somasundaram CK, Atchudan R, Edison TNJI, Perumal S, Vinodh R, et al. Sustainable synthesis of silver nanoparticles using marine algae for catalytic degradation of methylene blue. Catalysts. 2021;11:1377. https://doi.org/10.3390/catal11111377
53. Pallavicini P, Arciola C, Bertoglio F, Curtosi S, Dacarro G, et al. Silver nanoparticles synthesized and coated with pectin: An ideal compromise for anti-bacterial and anti-biofilm action combined with wound-healing properties. J Colloid Interface Sci. 2017;498:271-81. https://doi.org/10.1016/j.jcis.2017.03.062
54. Khawaja H, Zahir E, Asghar MA, Asghar MA. Graphene oxide, chitosan and silver nanocomposite as a highly effective antibacterial agent against pathogenic strains. Colloids Surf A Physicochem Eng Asp. 2018;555:246-55. https://doi.org/10.1016/j.colsurfa.2018.06.052
55. Chen R, Yang L, Guo Y, Zheng W, Liu H, Wei Y. Effect of p-nitrophenol degradation in aqueous dispersions of different crystallized goethites. J Photochem Photobiol A Chem. 2018;353:337-43. https://doi.org/10.1016/j.jphotochem.2017.11.028
56. Sun H, Zelekew OA, Chen X, Guo Y, Kuo DH, et al. A noble bimetal oxysulfide CuVOS catalyst for highly efficient catalytic reduction of 4-nitrophenol and organic dyes. RSC Adv. 2019;9:31828-39. https://doi.org/10.1039/C9RA05172D
57. Singh J, Mehta A, Rawat M, Basu S. Green synthesis of silver nanoparticles using sun dried tulsi leaves and its catalytic application for 4-nitrophenol reduction. J Environ Chem Eng. 2018;6:1468-74. https://doi.org/10.1016/j.jece.2018.01.054
58. Khoshnamvand M, Huo C, Liu J. Silver nanoparticles synthesized using Allium ampeloprasum L. leaf extract: characterization and performance in catalytic reduction of 4-nitrophenol and antioxidant activity. J Mol Struct. 2019;1175:90-6. https://doi.org/10.1016/j.molstruc.2018.07.089

CC BY